

Electronic Supplementary Information for: Dynamic self-organization in fire ant rafts underpins collective longevity and threat responsiveness.

Zachary T. White, Franck J. Vernerey

S1 Surface density analysis

To estimate density of the raft surface, we take images of the raft using the identical setup explained previously. To begin, we convert images to grayscale before measuring the intensity of the raft after applying a dynamic mask, to exclude any surrounding water. This yields the unadjusted intensity as a function of position and time $I(x, y, t)$. We perform a similar measurement but on a smaller region adjacent to the raft. This yields the background intensity of light reflected from the bottom of the container. We average this to provide a single background intensity value in time $I_o(t)$. Using this, we calculate the transmissivity as $T_c(x, y, t) = I/I_o$, where normalizing the intensity of the raft, allows us to adjust for any variations in light level, or between separate experiments (see Fig. S8 for setup). To reduce noise we blur this quantity using a 2-D convolution,

$$C(m, n) = \sum_p \sum_q W(p, q) T_c(m - p + 1, n - q + 1)$$

where T_c is the input to be convolved, and W is the kernel of size approximately $2\sigma \times 2\sigma$. We find the results to be insensitive to reasonable choices of W (Fig. S15). We do not convert measured transmission into density ρ , as high density clusters, which often grow three-dimensionally, significantly obscure transmission. Thus low T_c values likely underestimate ρ , which in part explains why the dense peak in Figs. 2A-B and Fig. S15 are narrower than the dilute peak. A transmission value of zero is never recorded due to reflected and background light reaching the camera.

S2 Particle image velocimetry

To characterize surface ant activity we obtain the Eulerian vector field of the raft surface during experiments using PIVlab Version 3.02, in MATLAB 2023b (see Fig. S9). In order to extract movement of just surface ants and minimize capturing changes in underlying raft shape, we extract video footage at short 1 sec intervals. Structural changes in raft shape typically occur on the scale of minutes whereas surface ants self-propulsion speed $v_0 = 2.813$ mm/s is orders of magnitude faster. To obtain sufficient spatial sampling we set the interrogation length to about a single ant length $\sigma = 2.93$ mm. A mask was then dynamically applied to exclude surrounding water from being analyzed. The analysis provided the instantaneous velocity field \mathbf{v} at every spatial point \mathbf{x} on the raft. Raw data was first validated using a standard deviation filter with a selected threshold of 8 std. followed by a local median filter to remove noisy vectors. Missing data was replaced through interpolation. Despite the high sampling rate, PIV analysis does capture structural raft motion to some extent, especially during periods of surface ant inactivity. Finally, the global average speed $\langle |\mathbf{v}| \rangle$ is then computed for each frame.

S3 Bridge & protrusion growth

We track bridge and protrusion growth by measuring their change in length over time from initiation until they begin to recede. Length is obtained by tracing line segments from the base to tip of the protrusion, where the base is taken approximately where the raft changes concavity. Examples of measured protrusions are shown in Fig. S12. The linear growth rate was determined by fitting a line using the least squares method (raw data presented in Fig. S13).

S4 Captions for supplementary movies

Caption for Movie S1. High speed video showing raw footage of a raft gradually dewetting over the duration of 190 min. The acquisition frame rate was 1 fps. Movie shown at approximately 3800x speed.

Caption for Movie S2. A time lapse video showing presence of a stationary cluster coexisting with active ants on the raft surface. The acquisition frame rate was 1 fps. Movie shown at approximately 700x speed.

Caption for Movie S3. Displays raw high-speed footage of a raft undergoing an air stimulus response study. The burst of air was provided for about 5 seconds, corresponding to $t = 25$ min within the video. The acquisition frame rate was 1 fps. Movie shown at approximately 300x speed.

Caption for Movies S4-S6. Displays raw high-speed footage of a raft undergoing water stimulus studies, where hot water ($40^{\circ}C$) is added to a condensed raft in Movie S4, cold water ($13^{\circ}C$) was added to a spread raft in Movie S5, and cold water ($13^{\circ}C$) is added to a condensed raft in Movie S6. The acquisition frame rate for all movies was 1 fps. Movies are shown at approximately 100x speed.

Caption for Movie S7. Displays raw footage of the stochastic emergence and growth of a protrusion. The acquisition frame rate was 0.5 fps. Movie shown at approximately 100x speed.

Caption for Movie S8. Displays raw footage of the growth of a bridge, following placement of a secondary protrusion. The acquisition frame rate was 0.5 fps. Movie shown at approximately 50x speed.

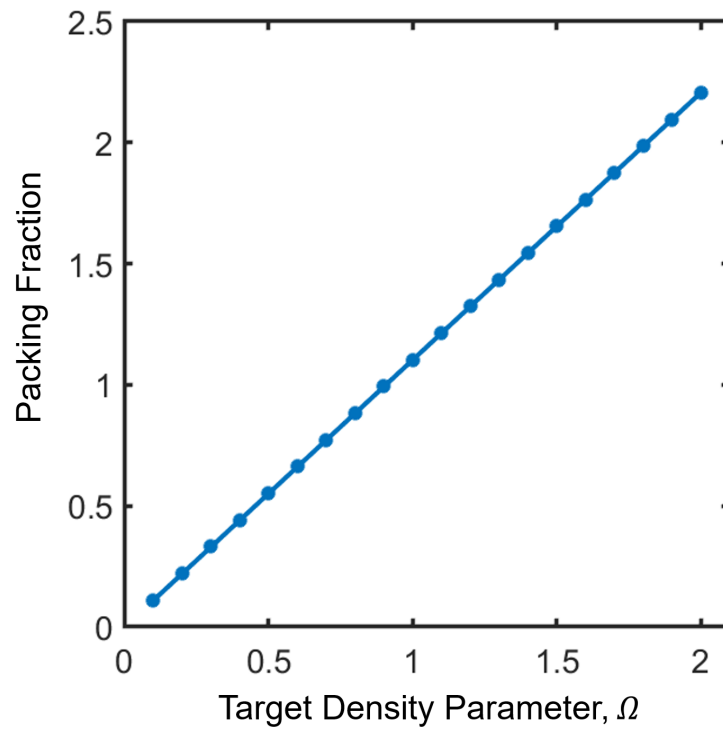


Figure S2: Treadmilling model surface packing fraction: Simulated packing fraction of ants on the raft surface at pseudo steady-state as computed by the ratio of free to structural ants with respect to the target density parameter $\Omega \in [0.1, 2]$. A packing fraction of 1.0 therefore corresponds to 1 surface ant per structural ant, which is achieved for $\Omega \sim 1$.

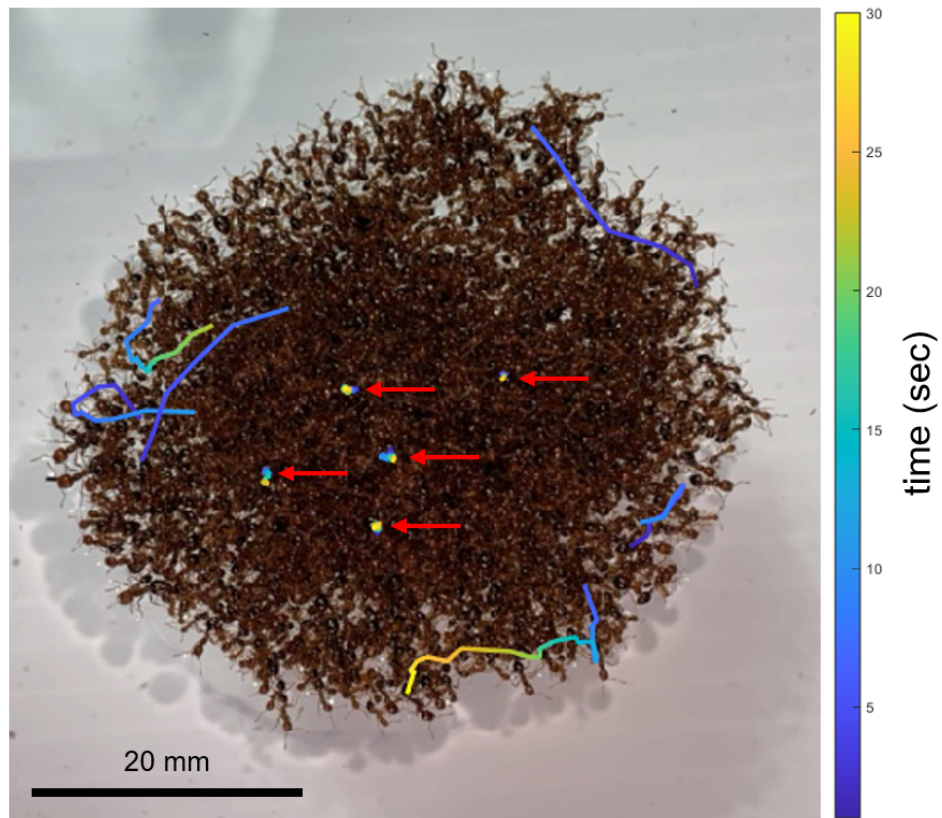


Figure S3: Trajectories of eleven ants on the raft surface, where color corresponds to the elapsed time at the ants particular location. Note that tracks do not necessarily begin at the same time as one another. We identify five ants (red arrows) within the cluster which remain nearly stationary over the complete 30 second duration. The remaining six ants, are observed to move freely across the raft surface. Tracks are ended early if ants becomes obscured or lost.

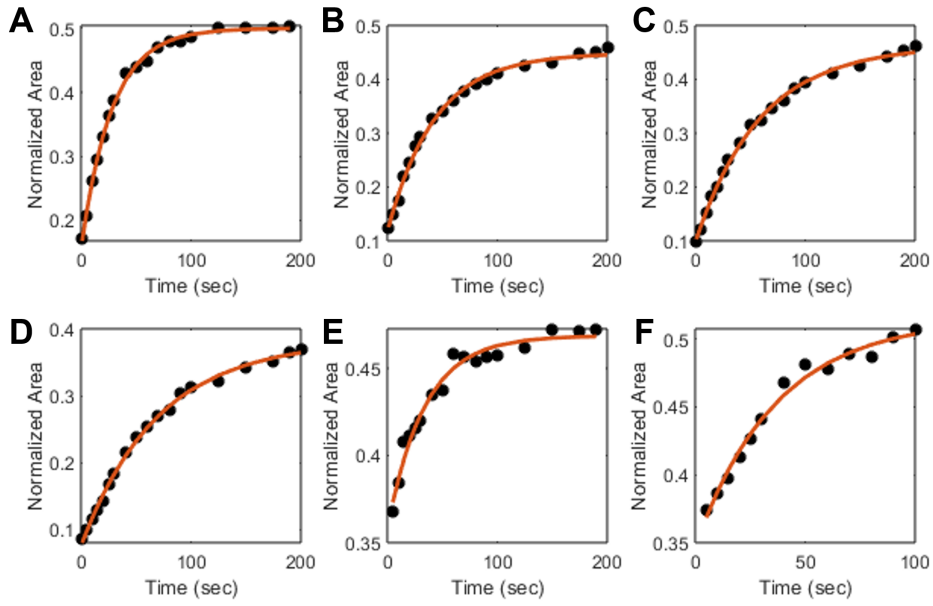


Figure S4: Raw change in normalized area A^* over time for rafts of size, (A) $N = 7000$ ants (B) $N = 3000$ ants (C) $N = 2000$ ants (D) $N = 1000$ ants (E) $N = 2000$ ants (F) $N = 2700$ ants. The characteristic timescale for wetting τ_w is determined by fitting an exponential (see Eqn. 13 in main text) by nonlinear least squares regression, shown in orange. Data presented in (A-D) is adapted from Mlot et al.(2011))

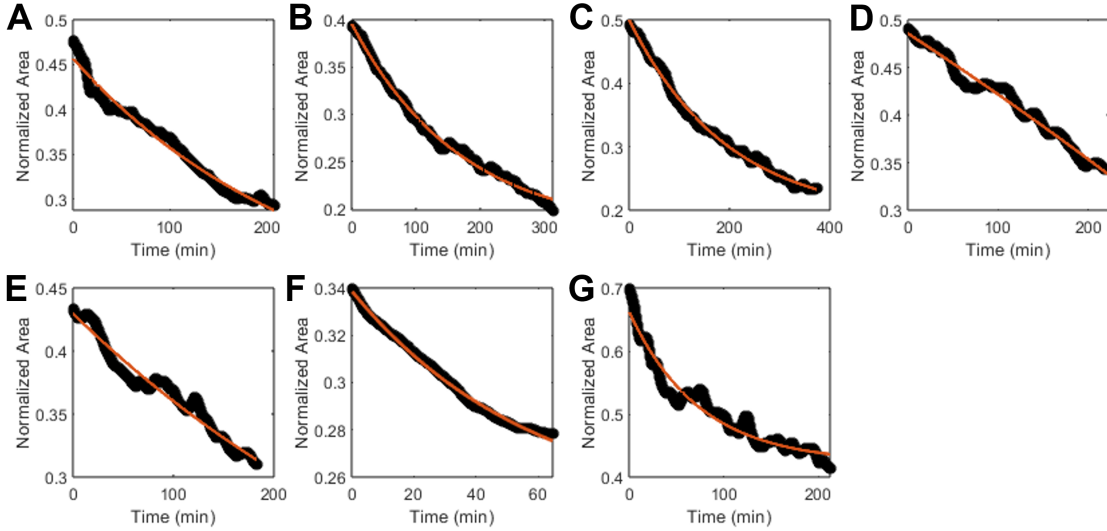


Figure S5: Raw change in normalized area over time for rafts of size, (A) $N = 2800$ ants (B) $N = 2800$ ants (C) $N = 2000$ ants (D) $N = 3600$ ants (E) $N = 3600$ ants (F) $N = 2000$ ants (G) $N = 400$ ants. The characteristic timescale for dewetting τ_{dw} is determined by fitting an exponential (see Eqn. 13 in main text) by nonlinear least squares regression, shown in orange.

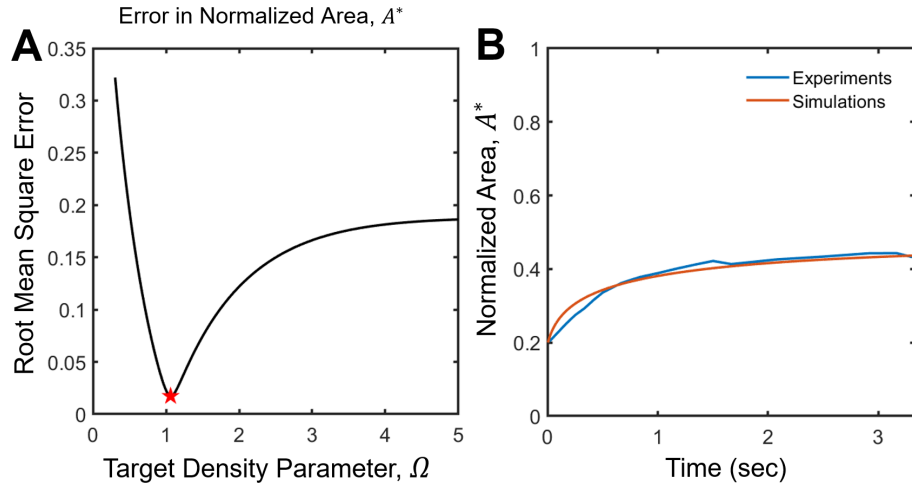


Figure S6: Simplified treadmilling model parameter sweep: Wetting. Results for the treadmilling model. (A) Plots of the root mean square error between simulated and experimental results shown with respect to $\Omega \in [0.1, 5]$. A value of $\Omega = 1.67$ was used to produce results in the main manuscript denoted by a red star and was chosen on the basis of minimum error. (B) Normalized area $A^*(t) = A(t)/(\frac{N}{\rho_s})$ over time for rafts wetting. The mean for $n = 6$ rafts is shown in blue. Simulation follows parameter chosen in (A)

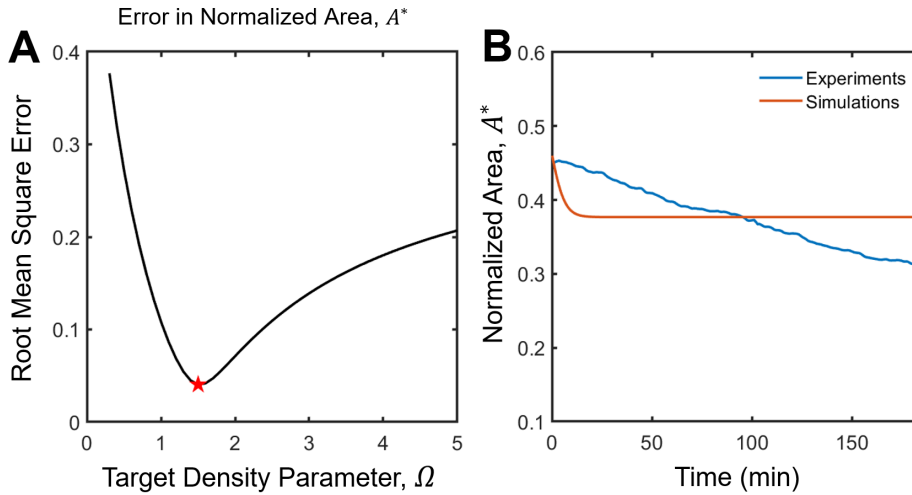


Figure S7: Simplified Treadmilling model parameter sweep: Dewetting. Results for the treadmilling model. (A) Plots of the root mean square error between simulated and experimental results shown with respect to $\Omega \in [0.1, 25]$. A value of $\Omega = 1.5$ was used to produce results in the main manuscript denoted by a red star and was chosen on the basis of minimum error. (B) Normalized area $A^*(t) = A(t)/(\frac{N}{\rho_s})$ over time for rafts wetting. The mean for $n = 5$ rafts is shown in blue. Simulation follows parameter chosen in (A)

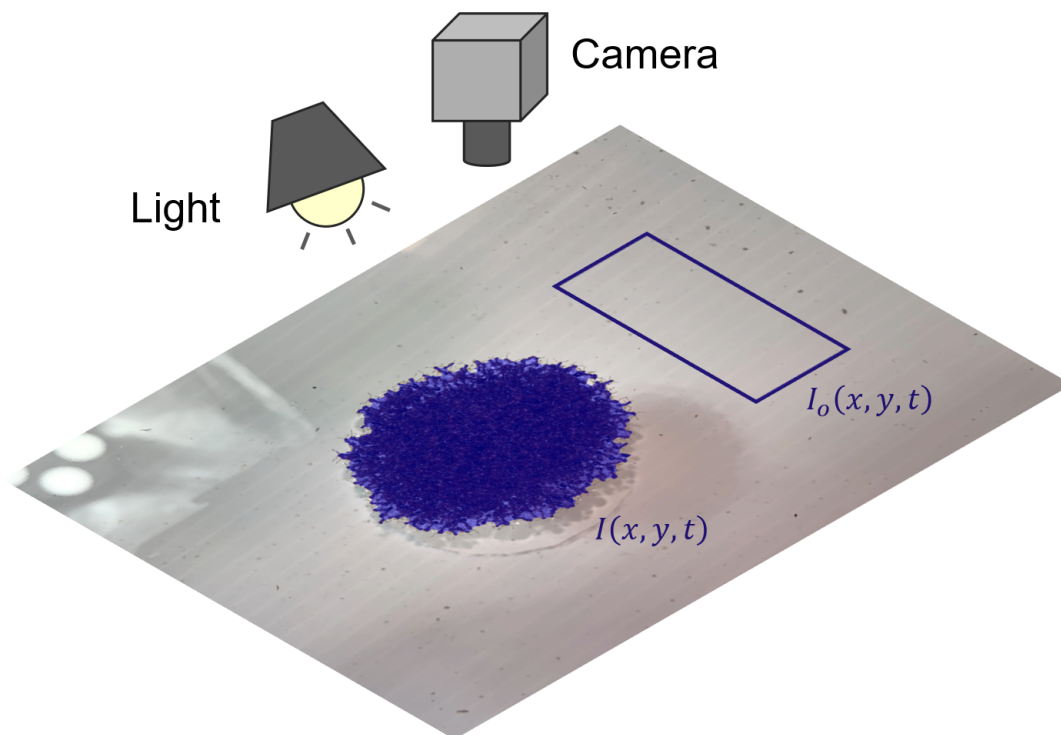


Figure S8: Raft Transmission Setup: Rafts are affixed to a vertical rod within a large container. A white plastic sheet is submerged at the bottom of the container providing a reflective background. Lights are placed above the raft directly behind the camera, and aimed towards the raft. A camera records the light transmitted through both regions. The first region $I(x, y, t)$ corresponds to the raft, and changes according to its shape through a dynamic mask, shown in blue. The second $I_o(x, y, t)$ is directly to the right of the raft and is used to normalize the data and compare between experiments.

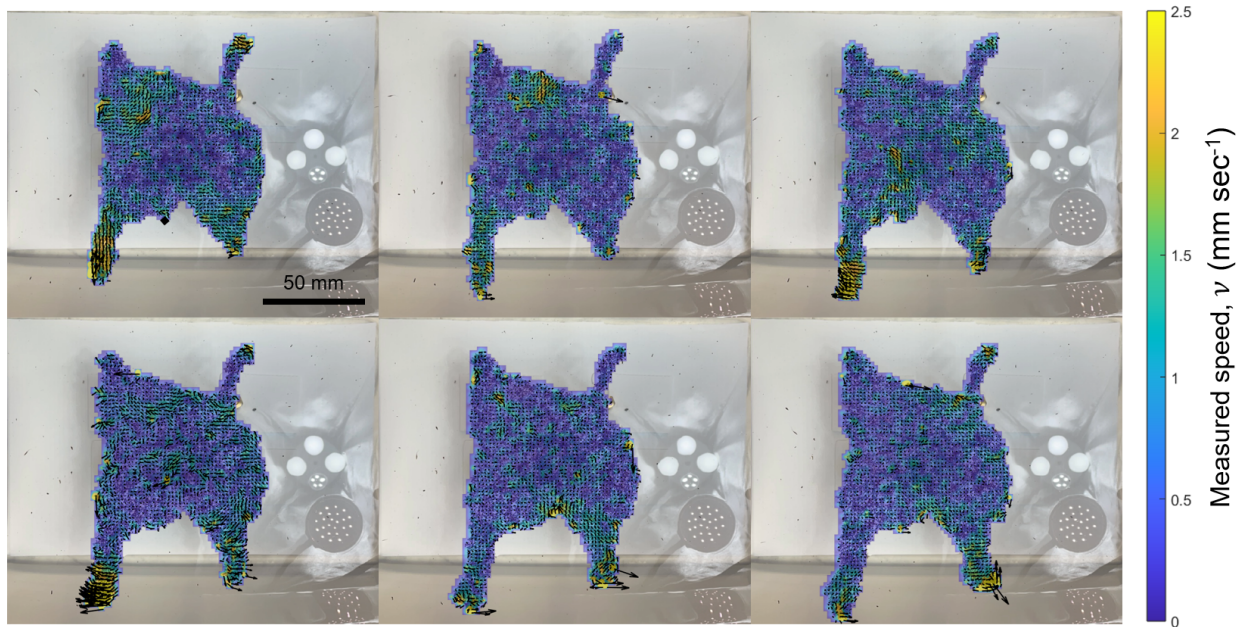


Figure S9: Heat maps of the measured speed, ν of the raft surface. Raft has about $N = 7000$ ants. The vector field represents the measured velocity at each grid point, where the interrogation length was set to the approximate length of a single ant $\sigma = 2.93$ mm. Panels are in approximately 100 sec intervals.

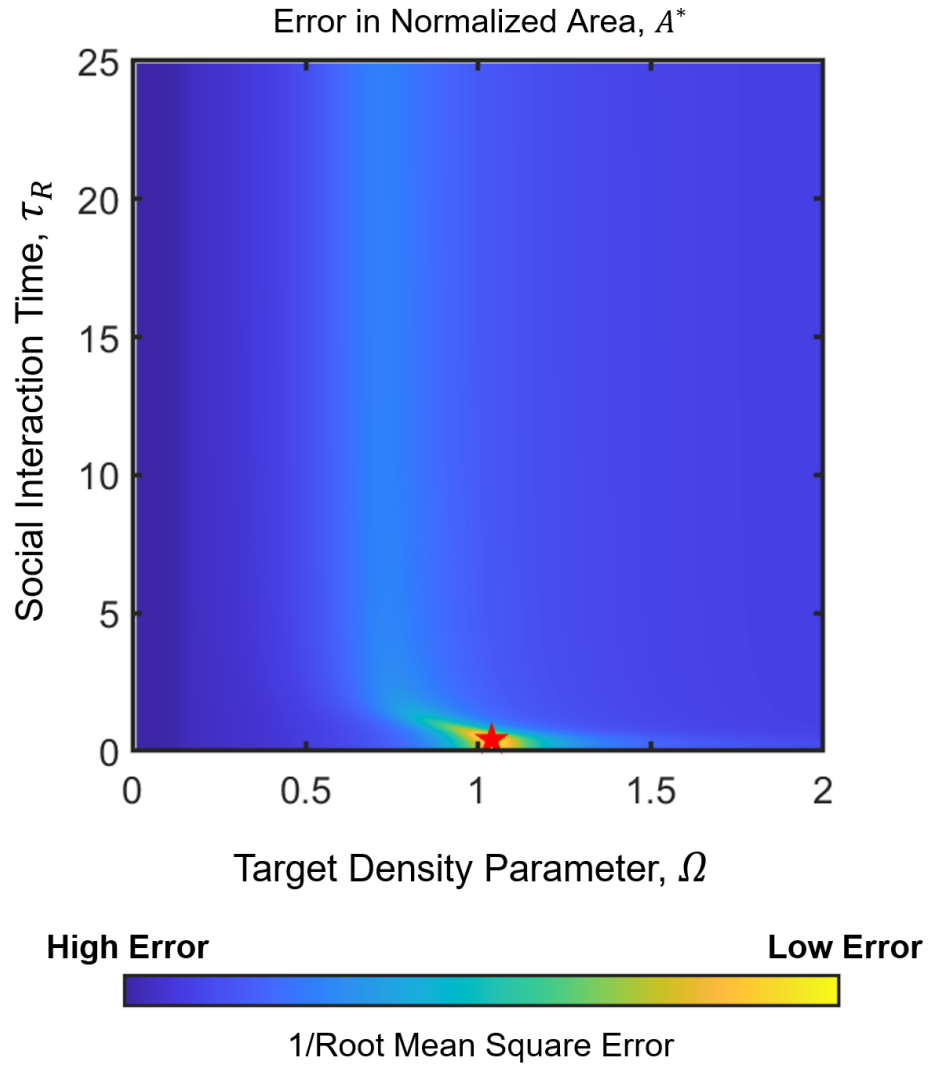


Figure S10: Parameter sweep phase space: Wetting. Phase plots of the the inverse root mean square error between simulated and experimental results for a raft wetting shown with respect to $\Omega \in [0.01, 2]$ and $\tau_R \in [0.01, 25]$ for the normalized area A^* . The parameters ($\Omega = 1.0$ and $\tau_R = 0.2$ sec) were used to produce results in the main manuscript denoted by a red star and was chosen on the basis of low error.

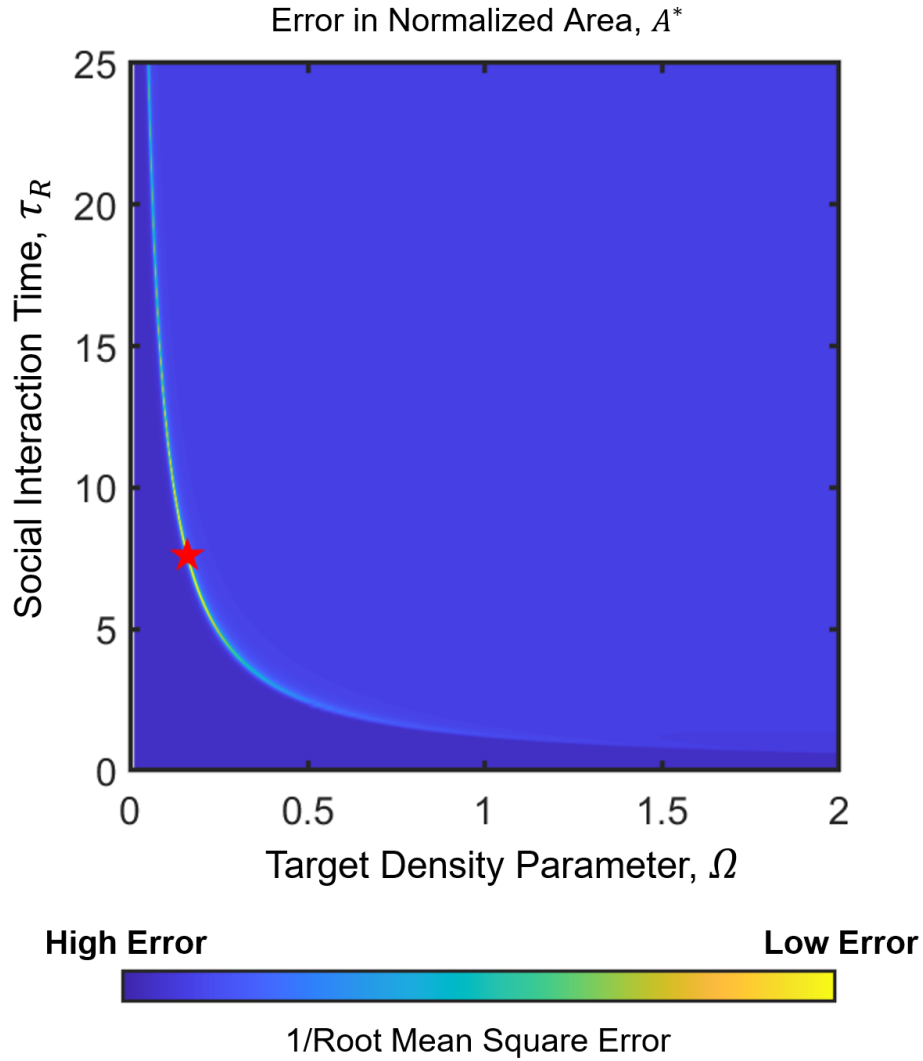


Figure S11: Parameter sweep phase space: Dewetting. Phase plots of the the inverse root mean square error between simulated and experimental results for a raft dewetting shown with respect to $\Omega \in [0.01, 2]$ and $\tau_R \in [0.01, 25]$ for the normalized area A^* . The parameters ($\Omega = 1.0$ and $\tau_R = 7.4$ sec) were used to produce results in the main manuscript denoted by a red star and was chosen on the basis of low error.

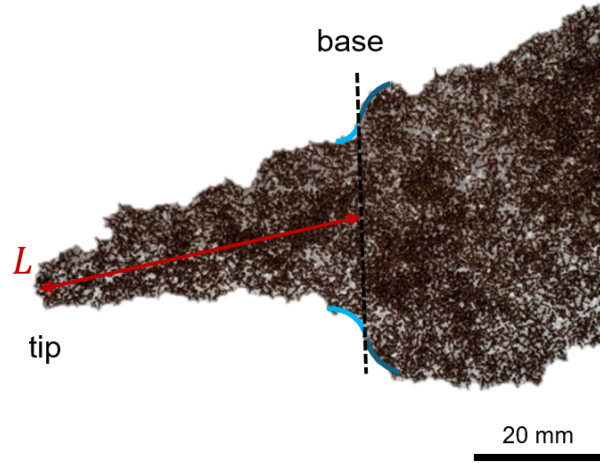


Figure S12: Measuring bridges and protrusions: Schematic illustrating length of a measured protrusion, where the length L is determined from taking a line segment from the tip to the base. The base is roughly taken as a line that intersects the inflection points (shown in grey) where the raft changes concavity from the protrusion (light blue) to the raft bulk (dark blue). Notice that while the raft edge is generally bumpy, changing concavity frequently, we generally consider the raft to change concavity when it spans the length of several ants.

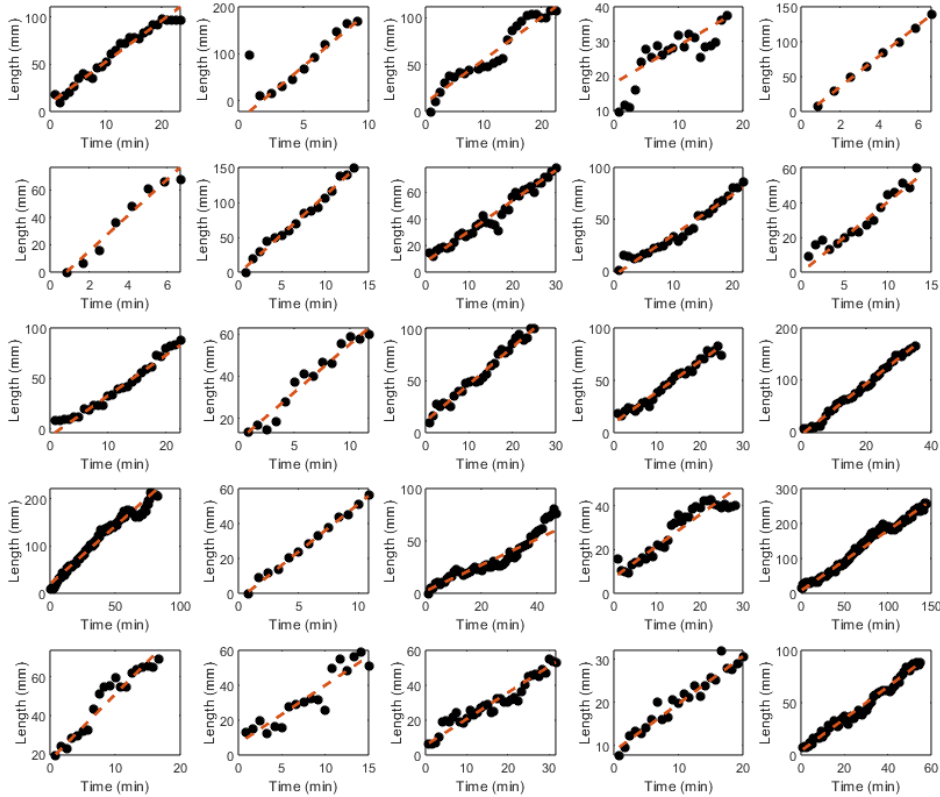


Figure S13: Raw change in length over time for protrusions and bridges. The linear growth rate is determined from a first order polynomial fit with least square error, shown in dashed orange.

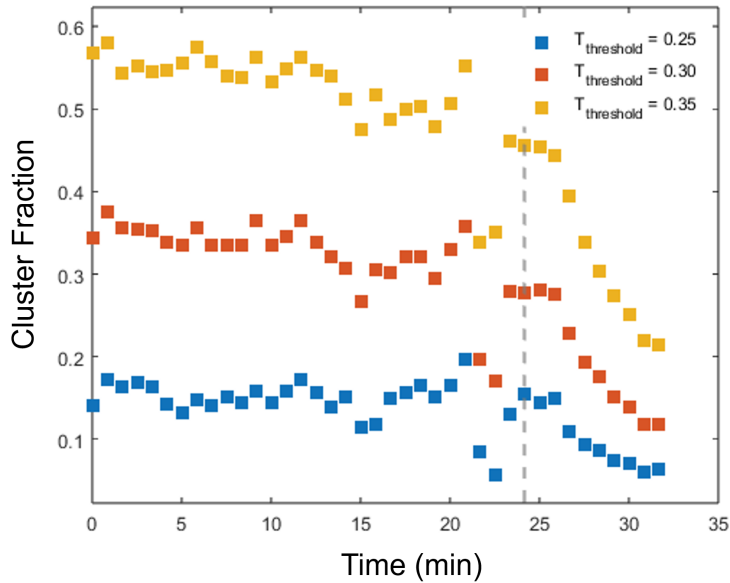


Figure S14: The cluster fraction with respect to time, for $T_{threshold} = 0.25$ (blue), $T_{threshold} = 0.30$ (orange), $T_{threshold} = 0.35$ (yellow). The emergence of a bridge is denoted by the dashed grey line. Recall that the threshold segments the transmission distribution, where values $T_c < T_{threshold}$ denote regions of the raft belonging to the cluster. Notice that changing the threshold has the effect of shifting the estimated cluster fraction, but not its overall trend. A value of $T_{threshold} = 0.30$ was used to produce results in the main manuscript.

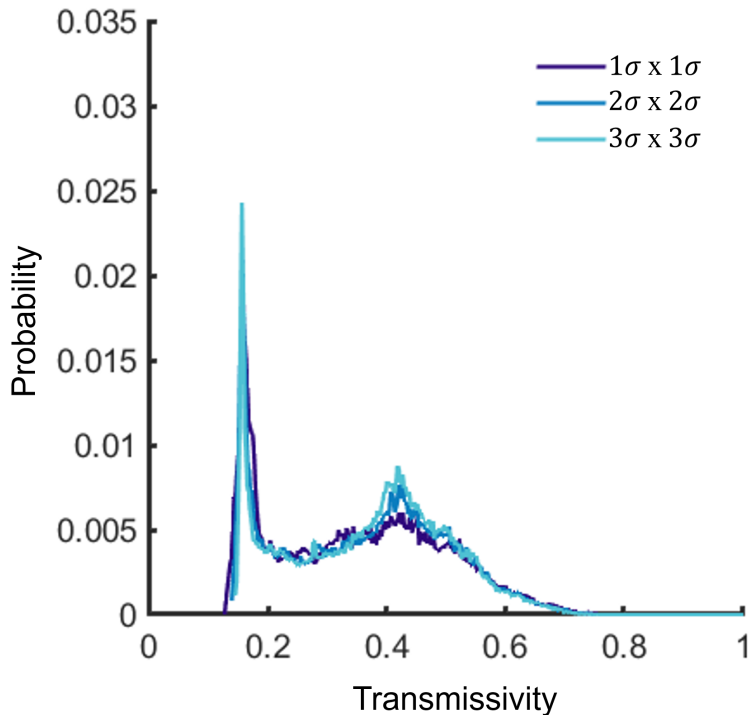


Figure S15: Sensitivity of measured transmission to convolution: Probability distribution of measured transmission for convolution kernel size $A = 1\sigma \times 1\sigma$ (dark blue), $A = 2\sigma \times 2\sigma$ (blue), $A = 3\sigma \times 3\sigma$ (light blue) where $\sigma \sim 2.93$ mm is the characteristic length of an ant. For the measured transmission shown above, 1σ corresponds to about 17 pixels, although this varies between trials. Recall that the kernel W is used to blur the measured transmission. Note that the distribution shape remains insensitive for reasonable choices of W .

Table 1: **Information for experimental trials.** Description of the experimental trials conducted, with the colony (1-6), the stimulus type used, and the date they were conducted.

Trial	Colony	Stimulus type	Date
1	2	None	07-Jul-2023
2	5	None	10-Jul-2023
3	4	None	11-Jul-2023
4	4	None	11-Jul-2023
5	1	None	12-Jul-2023
6	1	None	12-Jul-2023
7	5	None	13-Jul-2023
8	6	None	18-Jul-2023
9	5	None	23-Jul-2023
10	5	None	28-Jul-2023
11	3	Air	02-Aug-2023
12	3	Air	09-Aug-2023
13	3	Air	11-Aug-2023
14	3	Air	11-Aug-2023
15	2	Cold Water (13 °C)	31-Jul-2023
16	2	Cold Water (13 °C)	31-Jul-2023
17	3	Hot Water (40 °C)	09-Aug-2023
18	3	Hot Water (40 °C)	09-Aug-2023
19	3	Cold Water (13 °C)	09-Aug-2023
20	3	Cold Water (13 °C)	09-Aug-2023
21	3	Cold Water (13 °C)	09-Aug-2023
22	3	Cold Water (13 °C)	09-Aug-2023

Table 2: **Numerical model parameters for wetting-dewetting studies.** Simulation parameters values for both dewetting and wetting simulations described in the main manuscript.

Parameter	Description	Units	Dewetting	Wetting
Ω	Target density parameter	N/A	0.165	1.0
τ_R	Social interaction time	sec	7.4	0.2

Table 3: **Numerical model parameters for stimulus response studies.** Simulation parameters values prior, during, and after stimulus for both air and water stimulus-response simulations.

Initial Morphology	Stimulus Type	Parameter	Pre	Stimulus	Post
Clustered	Air	τ_R	7.4	[5,2.5,0.5]	7.4
Spread	Cold water	τ_R	1	20	1
		Ω	0.65	0.65	0.90
		δ	0.01	0.15	0.01
Clustered	Cold water	τ_R	7.4	20	7.4
		Ω	0.65	0.65	0.90
Clustered	Hot Water	τ_R	7.4	0.8	7.4
		Ω	0.165	0.165	0.60